

RSC Advances



This is an *Accepted Manuscript*, which has been through the Royal Society of Chemistry peer review process and has been accepted for publication.

Accepted Manuscripts are published online shortly after acceptance, before technical editing, formatting and proof reading. Using this free service, authors can make their results available to the community, in citable form, before we publish the edited article. This *Accepted Manuscript* will be replaced by the edited, formatted and paginated article as soon as this is available.

You can find more information about *Accepted Manuscripts* in the [Information for Authors](#).

Please note that technical editing may introduce minor changes to the text and/or graphics, which may alter content. The journal's standard [Terms & Conditions](#) and the [Ethical guidelines](#) still apply. In no event shall the Royal Society of Chemistry be held responsible for any errors or omissions in this *Accepted Manuscript* or any consequences arising from the use of any information it contains.

ARTICLE

Cite this: DOI:

Simultaneous improvement of strength and toughness in fiber reinforced isotactic polypropylene composites by shear flow and β -nucleating agent

Yan-Hui Chen,^a Zhang-Yong Huang,^b Zhong-Ming Li,^{a*} Jian-Hua Tang^b and Benjamin S. Hsiao^{c*}Received
Accepted

DOI:

www.rsc.org/

Inspired by the hierarchical structure of natural plants with a highly oriented and 'stiff' outer skin and an isotropic or poorly oriented 'soft' inner core, such as bamboo and sugarcane, we demonstrated an analogous hierarchical structure in glass fiber reinforced isotactic polypropylene (GF/iPP) composites with the aid of β -nucleating agent and oscillatory shear injection molding technique. The synthetic hierarchical structure consisted of composite assemblies of glass fibers and semi-crystalline matrix with self-reinforced crystalline shish-kebabs (α -crystals) throughout the molded part. It was found the outer layer was dominated by highly oriented glass fibers and shish-kebabs, while the inner layer contained less oriented glass fibers and shish-kebabs but a large population of β -crystals. As a result, the strength and toughness of the final GF/iPP parts were simultaneously improved (tensile strength was increased by 19.3 MPa and the impact toughness by two folds) compared to the conventional injection-molded GF/iPP parts. The approach exhibited a new pathway to further optimize the property of GF/iPP composites through structure manipulation.

Introduction

Glass fiber reinforced isotactic polypropylene (GF/iPP) composites have been widely used in electronics, automobiles, electrical appliances, etc., due to their excellent strength and toughness, high distortion temperature, good dimensional stability and attractive performance/cost ratio.¹⁻³ Under conventional processing conditions, iPP in the GF/iPP composites usually crystallizes into α -crystals, which possess relatively low strength, especially at low temperatures.^{4,5} Apart from that, the discrepancy of elastic modulus of glass fibers and iPP matrix, in conjunction with the weak interfacial adhesion, can also result in poor interfacial stress transfer in GF/iPP composites.⁶ As a result, conventionally processed GF/iPP composites often have relatively low impact toughness, which seriously restricts their application opportunities.⁷⁻⁹ Toughening of GF/iPP composites has thus become a major topic of interest for industrial applications.¹⁰⁻¹² Until now, two routes have been demonstrated to improve the toughness of GF/iPP composites. One is by blending of elastomers such as EPDM (ethylene-propylene-diene-monomer), SBS (styrene-butadiene-styrene) and SEBS (styrene-ethylene-butylene-styrene).¹⁰⁻¹² The other is by modifying the interface between glass fibers and iPP. In this case, the surface of glass fibers is treated by a silane coupling agent and the iPP matrix is also modified by addition of compatibilizers (e.g. octane-ethylene copolymer, maleic anhydride grafted octane-ethylene copolymer or maleic anhydride grafted iPP).^{13, 14} Although both routes are able to improve the impact toughness, they are also accompanied by some disadvantages including reduced strength and modulus, increased cost, and complicated procedures.^{10-12, 15-20}

It is well-known that iPP is a polymorphic semi-crystalline polymer that has four crystal modifications: α , β , γ and smectic.^{21, 22} Compared with other modifications, β -crystals received the most attention due to the excellent impact toughness and elongation at break.²³⁻²⁷ The excellent impact toughness of β -iPP is originated from the β - α polymorphous transition and the loose structure in β -crystals (compared with α -crystals) that are particularly capable of absorbing impact energy.²⁷⁻²⁹ Thermodynamically metastable β -crystals can only be obtained under special crystallization conditions, such as in the presence of β -nucleating agents,³⁰⁻³² in a temperature gradient,³³ or under a shear flow.^{34, 35} Among the above conditions, the approach of adding β -nucleating agent offers some practical advantages over the other ones. As the required loading of β -nucleating agent is very low, the practice does not alter the processing conditions and can lead to a high performance/cost ratio. Hence, β -nucleating agent was frequently added to iPP to improve the impact toughness of iPP. Tjong et al. reported that the impact fracture toughness of β -nucleated iPP could be increased by 100 % when compared to that of pure iPP.²⁴ Karger-Kocsis et al. evaluated the fracture mode of iPP by the method of three-point bending and also reported that the fracture energy of iPP containing β -nucleating agent was approximately twofold of the pure iPP.^{25, 36} The presence of β -nucleating agent in GF/iPP composites also exhibited the ability to toughen the system. For example, Xie et al. discovered that 1.0 wt % β -nucleating agent loading in GF/iPP composites could increase the impact toughness from 9.3 kJ/m² (without β -nucleating agent) to 14.6 kJ/m². However, the addition of β -nucleating agent decreased corresponding tensile strength and modulus slightly.³⁷ So far, it is still a

scientific challenge to improve the toughness of GF/iPP composites without sacrifice of strength and modulus.

Inspired by some plants in the natural world, such as bamboo and sugarcane that exhibit excellent overall mechanical properties due to their unique hierarchical structure (i.e., a highly oriented 'stiff' outer layer and an isotropic or a less oriented 'soft' inner core), we attempted to manufacture injection-molded GF/iPP parts also with a similar skin-core structure to simultaneously improve toughness as well as strength and stiffness. To realize this goal, we adopted the combined methods of β -nucleating agent addition and an advanced injection molding technique (oscillatory shear injection molding, OSIM) to prepare the GF/iPP parts. The OSIM technique is quite different from the conventional injection molding (CIM) technique, where its unique feature is that during OSIM processing, the hot melt in the mold is subjected to high pulse shear stress driven by two pistons moving reversibly at the same frequency.⁴ Thus, the processing of GF/iPP composites by OSIM technique could be divided into two stages. In the outer layer, the shear flow could generate highly oriented crystalline structures (i.e., self-reinforced shish-kebabs) and aligned glass fibers along the shear direction, where the efficiency of β -nucleating agent was very low since no β -crystals were seen.^{4, 38} However, in the inner core, the shear flow intensity decreased rapidly and imposed light effect on the orientation of glass fibers and iPP melt, where the β -nucleating agent became the dominant factor that induced a high fraction of β -crystals. The resulting GF/iPP composite thus possessed a unique hierarchical structure containing a strengthened skin and a toughened core. In other words, the outer layer consisted of self-reinforced crystalline shish-kebabs and highly oriented glass fibers, while the inner layer contained less oriented shish-kebabs and glass fibers but a tougher matrix dominated by β -crystals. This structure provided simultaneous improvement of impact toughness and tensile strength in the final GF/iPP parts.

Experimental

Materials

Isotactic polypropylene (iPP, model T30S) was purchased from Dushanzi Petroleum Chemical Co., China, with a melt flow rate (MFR) of 3 g/10 min (230 °C, 21.6 N), $M_w = 39.9 \times 10^4 \text{ g}\cdot\text{mol}^{-1}$, and $M_w/M_n = 4.6$. Chopped glass fiber with diameter of 13~17 μm (GF E-glass, ECS13-3-508, Jushi Group Co., Ltd, China) was used as received. The chosen β -nucleating agent was aryl amide compounds (TMB-5), which had a similar chemical structure as some aromatic amine β -phase nucleating agent, such as N,N'-dicyclohexyl-2,6-naphthalene dicarboxamide.^{32, 39} This compound was supplied by Fine Chemical Institute, Shanxi, China.

Sample preparation

The preparation scheme for making composite samples was as follows. Pellets of iPP and 30 wt % glass fibers, with and without 0.2 wt % β -nucleating agent, were melt mixed in a co-rotating twin screw extruder and pelletized. The screw speed was fixed at 82 rpm and the processing temperature profile was from 200 to 210 °C from hopper to die. The composite GF/iPP pellets were then injection molded into rectangular plates having dimensions of 60 × 60 × 4 mm³ using oscillatory shear injection molding (OSIM) technique (the injection temperature profile was from 200 to 210 °C from hopper to nozzle). The detailed information about the OSIM processing is available in

the Supporting Information. The conventional injection molding (CIM) was also used under the identical thermal conditions without oscillatory shear to prepare samples for comparison purpose. For convenience, the samples prepared by OSIM processing and CIM processing were designated as OSIM samples and CIM samples, respectively. Furthermore, the OSIM GF/iPP samples with and without 0.2 wt % β -nucleating agent were designated as OSIM β and OSIM0, respectively. Due to the skin-core structure in OSIM and CIM samples, the specimens were characterized layer by layer along the thickness direction.⁴⁰ In addition, the outer and inner layers were referred to the layers from the surface to ca. 1.0 mm in depth, and from 1.0 to 2.0 mm along the thickness direction, respectively.

X-ray measurements

Two-dimensional wide-angle X-ray diffraction (2D-WAXD) and two-dimensional small-angle X-ray scattering (2D-SAXS) measurements were carried out at the Advanced Polymers Beam line (X27C, $\lambda = 0.1371 \text{ nm}$) in the National Synchrotron Light Source (NSLS), Brookhaven National Laboratory (BNL). A MAR CCD X-ray detector (MARUSA) was employed for detection of 2D-WAXD and 2D-SAXS images, having a resolution of 1024 × 1024 pixels (pixel size = 158.44 μm). The sample-to-detector distance was 112.6 mm for WAXD (calibrated by an aluminum oxide (Al₂O₃) standard) and 2330 mm SAXS (calibrated by a silver behenate (AgC₂₂H₄₃O₂) standard), respectively. The scattered intensities were registered in the range of scattering angles 2θ from 5° to 25°.

Linear WAXD profiles were obtained from circular integration of intensities from 2D-WAXD images. The intensity was plotted as a function of the scattering vector, q , where $q = 4\pi \sin\theta/\lambda$ with λ being the wavelength of the incident beam, and 2θ being the scattering angle. Subsequently, through deconvolution of the diffraction peaks in linear WAXD profiles, the overall crystallinity X_c was calculated using the following expression:

$$X_c = \frac{\sum A_{\text{cryst}}}{\sum A_{\text{cryst}} + \sum A_{\text{amorp}}} \quad (1)$$

where A_{cryst} and A_{amorp} are the fitted areas of the crystal and amorphous peaks, respectively. The relative amount of β -crystals, K_β , was evaluated using the method of Turner-Jones.⁴¹

$$K_\beta = \frac{A_\beta(110)}{A_\beta(110) + A_\alpha(110) + A_\alpha(040) + A_\alpha(130)} \quad (2)$$

where $A_\beta(110)$ represents the area of the (110) reflection peak of β -crystals; $A_\alpha(110)$, $A_\alpha(040)$ and $A_\alpha(130)$ are the areas of the (110), (040), (130) reflection peaks of α -crystals, respectively.⁴² Meanwhile, the crystallinity of β -crystals X_β was given by

$$X_\beta = K_\beta X_c \quad (3)$$

More details about WAXD data analysis are available in references.^{35, 43}

Herman's method was used to determine the degree of orientation for lamellar crystals in the injection-molded parts.⁴⁴ In this method, the crystalline orientation was characterized by the average orientation of the normal to the crystalline plane with respect to an external reference frame. Accordingly, the flow direction was taken as the reference direction. For a set of hkl planes,

the average orientation, expressed as $\langle \cos^2 \Phi \rangle_{hkl}$, was calculated mathematically using the following equation:

$$\langle \cos^2 \Phi \rangle_{hkl} = \frac{\int_0^{\pi/2} I(\Phi) \cos^2 \Phi \sin \Phi d\Phi}{\int_0^{\pi/2} I(\Phi) \sin \Phi d\Phi} \quad (4)$$

with Φ being the azimuthal angle and $I(\Phi)$ being the scattered intensity along the angle Φ . Herman's orientation function, f , was defined as

$$f = \frac{3 \langle \cos^2 \Phi \rangle_{hkl} - 1}{2} \quad (5)$$

with f having a value of -0.5 with the normal of the reflection plane being perpendicular to the reference direction ($\Phi = 90^\circ$), a value of 1 with the normal of the reflection plane parallel being the reference direction ($\Phi = 0^\circ$), and a value of 0 with the orientation being random. For evaluation of the degree of orientation, the azimuthal intensity distribution $I(\Phi)$ at $q = 1.20 \text{ \AA}^{-1}$ was analyzed. This peak represented the (040) reflection of α -crystals in iPP, which only appeared at the equator in the WAXD patterns once oriented. The value of f was ranged from 0 to 1 due to the diffraction characteristics of (040) lattice plane, where the value of f increased from 0 to 1, indicating that crystal reflection plane changed from random orientation to full alignment along the flow direction.

Differential scanning calorimetry (DSC)

DSC measurements were carried out using the TA DSC Q20 instrument with a constant heating rate of $10 \text{ }^\circ\text{C}\cdot\text{min}^{-1}$ under a nitrogen atmosphere. The data were collected from 40 to $200 \text{ }^\circ\text{C}$ for each thermal scan, and the sample weight was kept in the range between 5 and 10 mg.

Scanning electronic microscopy (SEM)

The cryogenically fractured composite samples were prepared in liquid nitrogen by bending the samples along the shear flow direction (FD). The fractured sample was coated by gold sputtering, the distribution of the fiber and its adhesion with the iPP matrix were investigated using a SEM instrument, JSM-5900LV, operating at 20 kV. In order to study the crystalline morphology, the test specimen were cryogenically fractured in liquid nitrogen, and subsequently etched by 1% solution of potassium permanganate in a mixture of sulphuric acid, 85% orthophosphoric acid and water for 40 hours. The etched surface was then covered by gold sputtering and observed by a SEM instrument (Inspect F, FEI Company) operating at 20 kV.

Mechanical property tests

The tensile and impact specimens with a dimension of $60 \times 6 \times 4 \text{ mm}^3$ were machined from the injection-molded samples. The tensile test was performed at $23 \text{ }^\circ\text{C}$ and a crosshead speed of $50 \text{ mm}\cdot\text{min}^{-1}$ according to ASTM D-638. The notched impact test was carried out at $23 \pm 2 \text{ }^\circ\text{C}$ based on ASTM D256-05 with a V-notch of a 1.2 mm depth. The values of all the mechanical parameters were calculated as averages over 5 samples for each test.

Results and discussion

Mechanical properties

Fig. 1 shows the mechanical properties of all four GF/iPP composite samples. For the conventional injection-molded GF/iPP samples, the addition of β -nucleating agent in the GF/iPP composite (CIM β) slightly decreases the tensile strength and modulus, but moderately increases the impact strength. The tensile strength and modulus decrease from 39.2 MPa and 2.1 GPa for non-nucleated GF/iPP composite (CIM0) to 39.0 MPa and 1.9 GPa, respectively, but the impact strength rises from 6.6 kJ/m^2 to 7.2 kJ/m^2 . The presence of β -nucleating agent in the CIM β sample induces the formation of β -crystals, which accounts for the decreases in tensile strength as well as modulus and increase in impact strength. The same trend has also been observed in previous studies on using β -nucleating agents to toughen the iPP composites.^{37, 45-47}

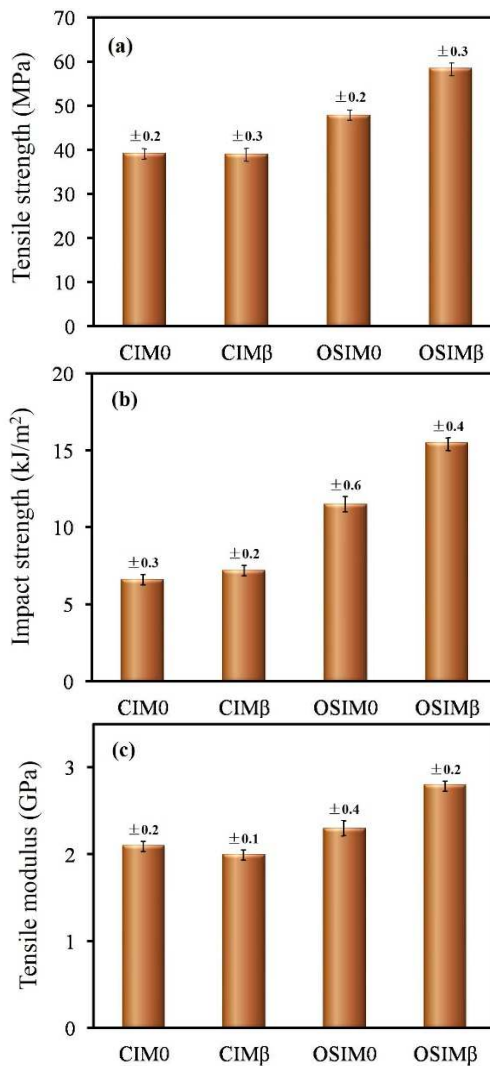


Fig. 1. Mechanical properties of GF/iPP composites and β -nucleated GF/iPP composites: (a) tensile strength, (b) impact strength, and (c) tensile modulus. (CIM0: conventional injection molded GF/iPP composite with 30 wt% glass fibers; CIM β : conventional injection molded GF/iPP composite with 30 wt% glass fibers and 0.2 wt% β -nucleating agent; OSIM0: oscillatory shear injection molded with 30 wt% glass fibers; OSIM β : oscillatory shear injection molded with 30 wt% glass fibers and 0.2 wt% β -nucleating agent.)

ARTICLE

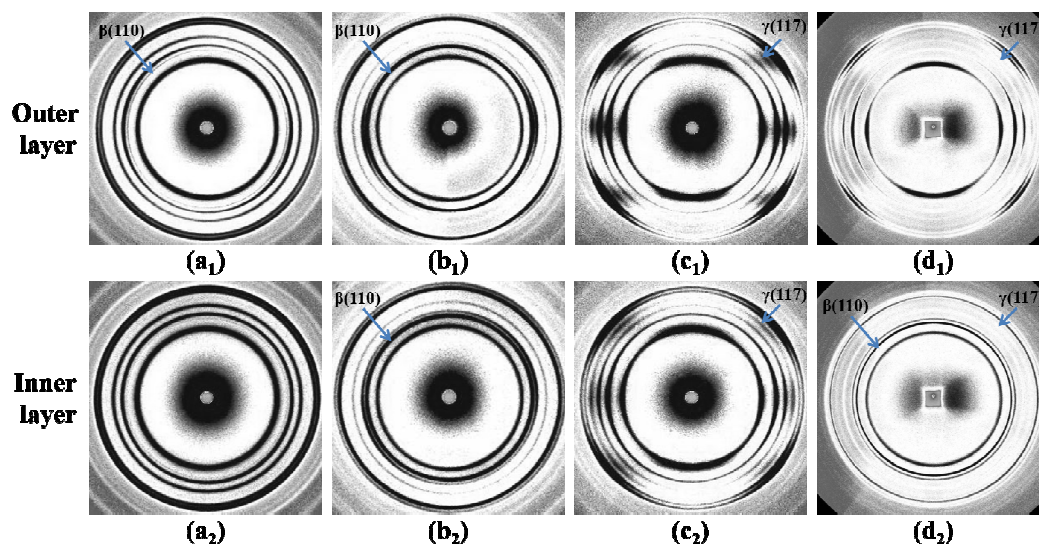


Fig. 2. Selected 2D-WAXD patterns of (a1-a2) CIM0, (b1-b2) CIM β , (c1-c2) OSIM0 and (d1-d2) OSIM β . The subscripts, 1, 2 represent the position of the sample, whose distance to the surface along the thickness is 0.4 (outer layer), 2.0 (inner layer) mm, respectively. The shear flow direction (FD) is vertical.

It is also shown that OSIM samples (OSIM0 and OSIM β) exhibit superior tensile strength, tensile modulus and impact strength to the CIM samples (CIM0 and CIM β) in Fig. 1. Moreover, it is interesting to note that the addition of β -nucleating agent to the oscillatory shear injection-molded GF/iPP sample (OSIM β) not only gives rise to higher tensile strength and modulus, but also improves impact strength, when compared to non-nucleated GF/iPP sample (OSIM0). To be specific, the tensile strength of the OSIM β sample reaches 58.5 MPa, an increase of 19.3 MPa compared to that of the CIM0 sample (39.2 MPa), while the impact strength of the OSIM β sample (15.5 kJ/m²) is over two times of that of the CIM0 sample (6.6 kJ/m²). In addition, the tensile modulus rises from 2.1 GPa to 2.80 GPa. Hence, we could conclude that the simultaneous reinforcement and toughening of the GF/iPP composites have been successfully achieved through the addition of β -nucleating agent and the use of oscillatory shear flow. The following sections systematically discuss the hierarchical structure and morphology of the OSIM β sample by means of WAXD, DSC, SAXS and SEM, in order to reveal the origin underlying the simultaneously reinforced and toughened GF/iPP composites.

Crystalline structure and molecular chain orientation

Fig. 2 shows the selected 2D-WAXD patterns from different layers, viz. inner and outer layers. The diffraction intensity distribution of CIM0 sample consists of five basic diffraction rings associated with different lattice planes of iPP, including (110), (040), (130), (111), and (-131), from inner to outer layers, respectively, which are characteristics of α -crystals. An additional weak (110) lattice plane also appears, corresponding to the reflection of β -crystals in the outer layer (Fig. 2a₁). It can be found that the diffraction peak of β -crystals emerges in outer

and inner layers of the CIM0 sample, as evident in Fig. 3a. Due to short shearing duration and fast relaxation, the real content of β -crystals is quite low at a negligible level (not listed in Table 1). Moreover, the arc-like diffraction of α (040) lattice plane is clearly seen, indicative of molecular chain orientation of iPP, but it disappears in the inner layer (Fig. 2a₂). The degree of orientation also has a low level, about 0.783 at the position of surface, then, decreases from the outer to inner layer. It is negligible in the inner layer, so the value is zero (Table 2). The presence of β -crystals and molecular orientation is intimately correlated with the processing conditions where shear flow field exists.^{34, 35, 48} Generally, during the CIM processing, the oriented iPP melt caused by the shear flow field during the injection stage gives rise to molecular orientation structure; On the other hand, it also generates the development of a few α -row-nuclei, then a subsequent growth of the β -crystals on the formed α -row nuclei. Therefore, the appearance of β -crystals and the molecular orientation in the outer layer are reasonable results. Although the shear flow is also existent in the inner layer, the slow solidifying rate leaves enough time for relaxation of extended iPP chains, and eventually iPP melt crystallized in α -crystals without molecular orientation.

The pronounced diffraction intensity of β (110) lattice plane is seen in the outer and inner layers of the CIM β sample in Fig. 2b₁₋₂, due to the addition of β -nucleating agent. Clear characterization is further displayed in Fig. 3b. The real content of β -crystals approaches 0.5 (the relative amount of β -crystals is about 0.86) from the outer to inner layer (Table 1), suggestive of the high efficiency of β -nucleating agent. Analogous to the decreased trend in the degree of orientation of the CIM0 sample, the degree of orientation of the CIM β sample also declines from the outer to inner layer, ranging from 0.781 to 0 (Table 2).

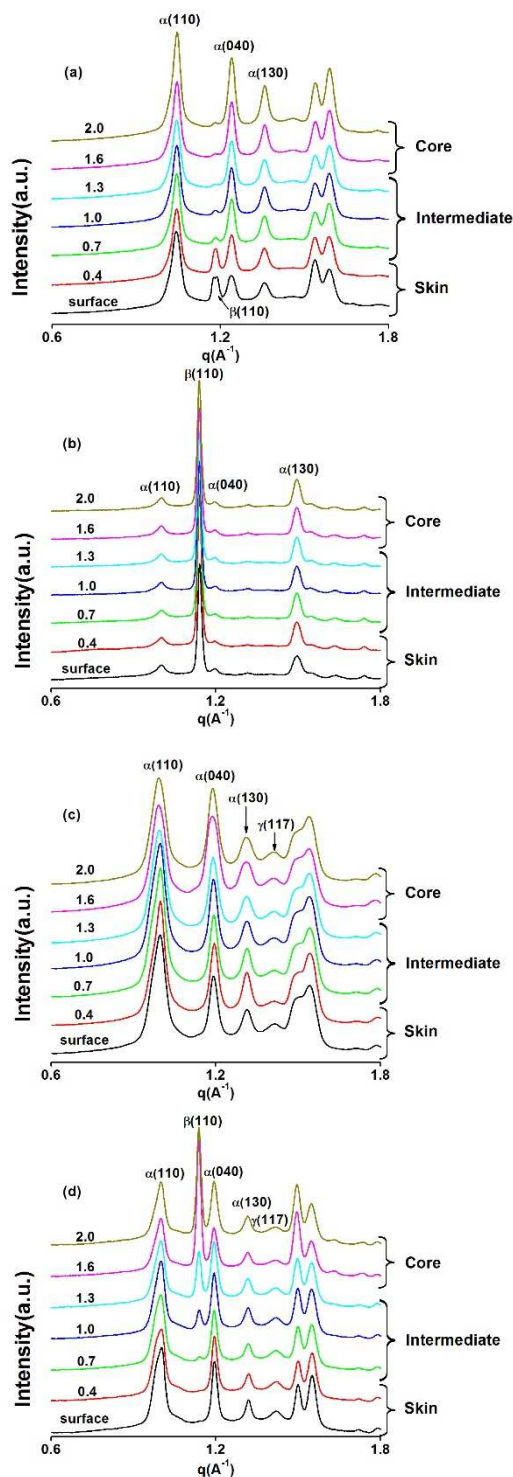


Fig. 3. Linear WAXD curves of (a) CIM0, (b) CIM β , (c) OSIM0 and (d) OSIM β obtained from circularly integrated intensities of 2D-WAXD patterns.

Compared with the CIM samples, distinct azimuthal diffraction intensity demonstrating strong molecular chain orientation is displayed in the outer and inner layers of the OSIM samples (Fig. 2c₁₋₂ and 2d₁₋₂). The degree of orientation of both OSIM samples is then calculated, as listed in Table 2. Their values are rather high, basically over 0.9, throughout the OSIM samples, although the degree of orientation of the OSIM

samples decreases marginally (from 0.972 to 0.921 for OSIM0; from 0.963 to 0.832 for OSIM β). Based on the peculiar feature of the OSIM technique, this strong molecular orientation throughout both OSIM samples is undoubtedly originated from the continuous oscillation shear on the melt. The slight reduction is due to the moderate relaxation of oriented molecular chains when the shear flow attenuates. Otherwise, at the fixed position the degree of orientation of the OSIM β sample is correspondingly lower than that of the OSIM0 sample, which indicates that the presence of β -nucleating agent to some extent weakens the orientation of molecular chains. According to the basic principle of shear flow-induced β -crystals,^{34, 35} β -crystals are supposed to form in the OSIM0 sample. On the contrary, almost no β -crystals appear in any layer of the OSIM0 sample (Fig. 2c₁₋₂ and Fig. 3c). This is quite associated by the complicated processing conditions. Although it is not in the scope of the present study, further work is planned to clarify the reason for the absence of β -crystals in the OSIM0 sample. It is interesting to note that strong reflections of β -crystals are almost absent in the outer layer, but apparently present in the inner layer of the OSIM β sample (indicated by an arrow in Fig. 2d₂ and more clearly in Fig. 3d). The real content of β -crystals increases from 0.027 to 0.224 (Table 1), and the fraction accordingly occupies from 4% to 39% of the total crystallinity (0.580) from the outer to the inner layer. At first, the continuous oscillation shear flow completely suppresses the effect of β -nucleating agent, causing the absence of β -crystals in the outer layer. In the inner layer where the shear flow attenuates, β -nucleating agent takes effect to induce abundant β -crystals. However, the content of β -crystals cannot be comparable to that in the CIM β sample (Table 1), due to the suppression of strong shear flow during the OSIM processing. Here, it is revealed the OSIM technique generated a hierarchical structure in the OSIM β sample, in which a great amount of molecular chain orientation structures formed throughout the whole OSIM β sample and abundant β -crystals only appeared in the inner layer. It can be deduced that the former is contributed to the enhanced strength, while the latter accounts for the increased toughness.

Table 1. β -Crystal Fraction Obtained from Linear-WAXD (Fig. 3).

position	depth from surface (mm)	CIM β	OSIM β
Outer layer	surface	0.443	0
	0.4	0.452	0
	0.7	0.432	0
Inner layer	1.0	0.458	0.027
	1.3	0.458	0.084
	1.6	0.460	0.182
	2.0	0.443	0.224

Table 2. Degree of Orientation Fitted From the Intensity of α (040) along Azimuthal Angle.

position	depth from surface (mm)	CIM0	CIM β	OSIM0	OSIM β
Outer layer	surface	0.783	0.781	0.942	0.963
	0.4	0.721	0.731	0.972	0.953
	0.7	0.623	0.643	0.953	0.932
Inner layer	1.0	0	0	0.935	0.944
	1.3	0	0	0.933	0.920
	1.6	0	0	0.934	0.866
	2.0	0	0	0.921	0.832

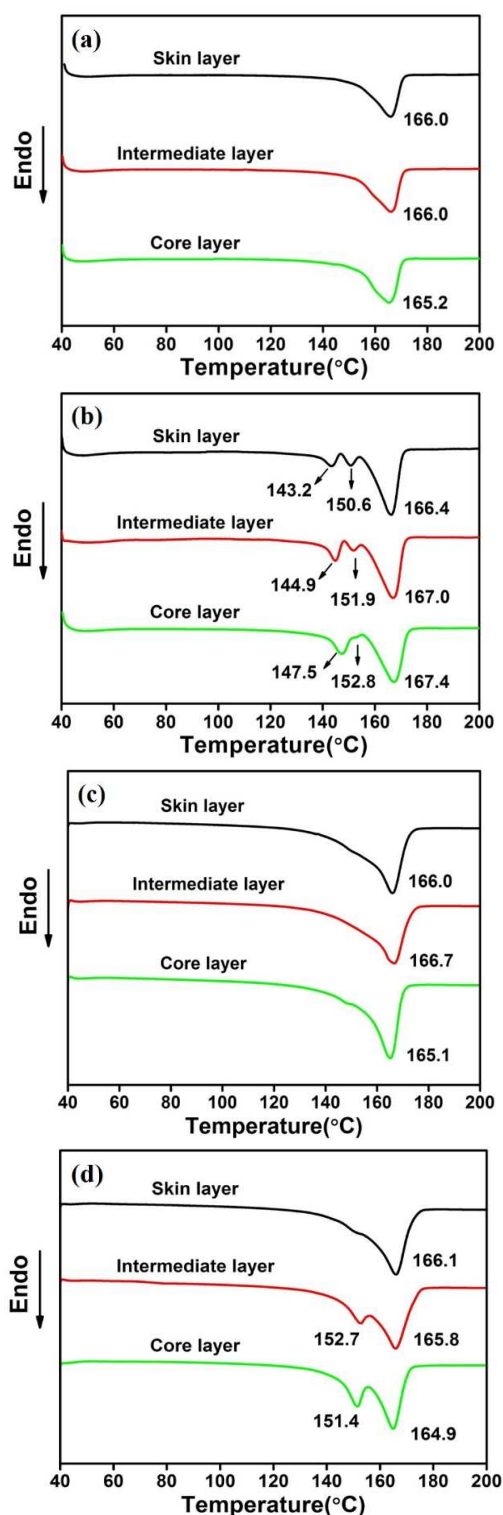


Fig. 4. DSC heating curves of (a) CIM0, (b) CIM β , (c) OSIM0 and (d) OSIM β .

It is worth noting that arcs of the γ -crystals appear at the diffraction patterns for the OSIM samples as well (Fig. 2c and 2d). This tiny amount of γ -crystals is clearly visible in Fig. 3c and 3d as the broad (117) peak after (130) peak. It was reported that the occurrence of γ -phase was mainly associated with high

molecular orientation and high pressure.⁴⁹ In our case, the appearance of γ -crystals in the OSIM samples can be ascribed to a combination of the local high pressure and shear.

Thermal behavior

In order to further verify the preferred distribution of β -crystals in the OSIM β sample, its thermal behavior was investigated by DSC measurement. The CIM0 and OSIM0 samples (Fig. 4a and 4c) only exhibit one endothermic peak of α -crystals at around 166 °C. In the case of CIM β sample, both layers show multi-endothermic peaks, one for α -crystals at around 166 °C and the other two for β -crystals between 150 and 153 °C (Fig. 4b).²⁷ An interesting phenomenon is observed in the OSIM β sample. There is only one endothermic peak of α -crystals (about 166.1 °C) in the outer layer, while an additional endothermic peak for β -crystals (about 151.4 °C) appears in the inner layer. This is in perfect agreement with the above WAXD results, which once again verifies that β -crystals are first suppressed by the intense shear field in the outer layer, but later induced by the revived β -nucleating agent in the inner layer.

Glass fiber orientation

As pointed out by WAXD measurement above, molecular orientation structure formed throughout the whole OSIM β sample. To get a comprehensive insight that whether the molecular orientation structure belongs to shish-kebab morphology, SAXS measurement was employed. It can be observed that strong intensity streaks distribute along the azimuth in the CIM samples (Fig. 5a and 5b). Normally, this kind of sharp streaks is considered to correspond to shish structure in almost all studies concerning flow-induced polymer crystallization.^{50, 51} In our case, it seems impossible since there are no adequate conditions for the formation of well-defined shish structure upon CIM processing. To our best of knowledge, in addition to characterizing the formation of lamellar orientation, SAXS measurement can also reflect distribution of longitudinal voids in fiber/polymer composites in real space.^{52, 53} We believe that the voids at the nano-scale level existing in the interface between glass fibers and iPP matrix contribute to these intensity streaks. More importantly, these randomly distributed intensity streaks, especially in the inner layer (Figure 5a₂ and 5b₂), indirectly indicate the random distribution of glass fibers. With regard to the OSIM samples, the typical shish-kebab patterns consisting of two clear scattering streaks display along and normal to the flow direction in Fig. 5c and 5d. Based on the results of the CIM samples, we consider that the increased equatorial streak intensity is attributed to the superposition of shish structure and nano-scale voids between glass fibers and iPP matrix. And these nano-scale voids are aligned perpendicularly to the flow direction, which reflects that the alignment of glass fibers along the flow direction. The SAXS patterns, in conjunction with 2D-WAXD patterns, demonstrate that under the influence of the intense shear flow, on one hand, nano-scale shish-kebab structure (molecular chain orientation structure mentioned in 2D-WAXD results) is on large scale formed upon OSIM processing; on the other hand, glass fibers mostly align along the flow direction.

ARTICLE

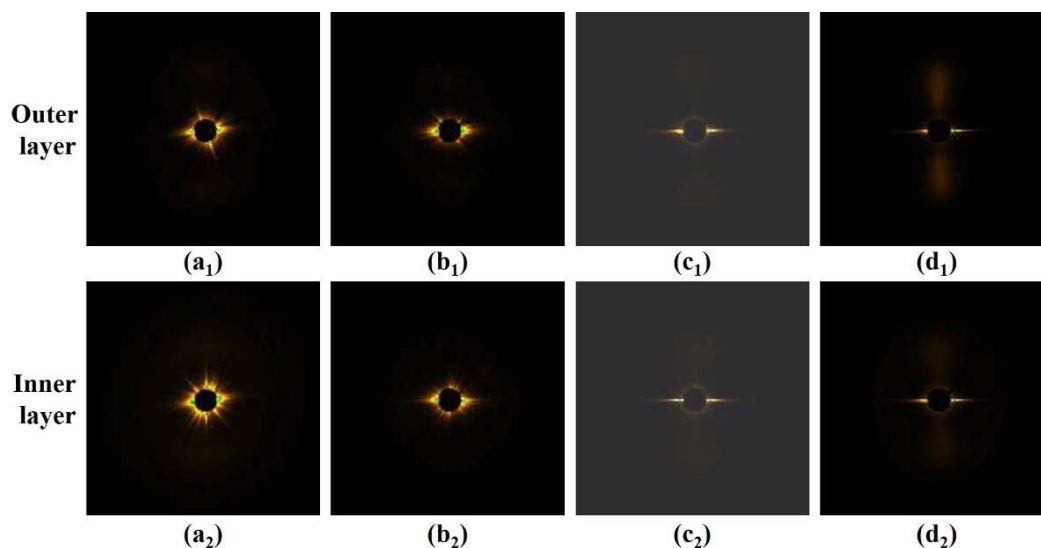


Fig. 5. Selected 2D-SAXS patterns of (a₁-a₂) CIM0, (b₁-b₂) CIM β , (c₁-c₂) OSIM0 and (d₁-d₂) OSIM β . The subscripts, 1 and 2, represent the position of the sample, whose distance to the surface along the thickness is 0.4 (outer layer) and 2.0 (inner layer) mm, respectively. The shear flow direction (FD) is vertical.

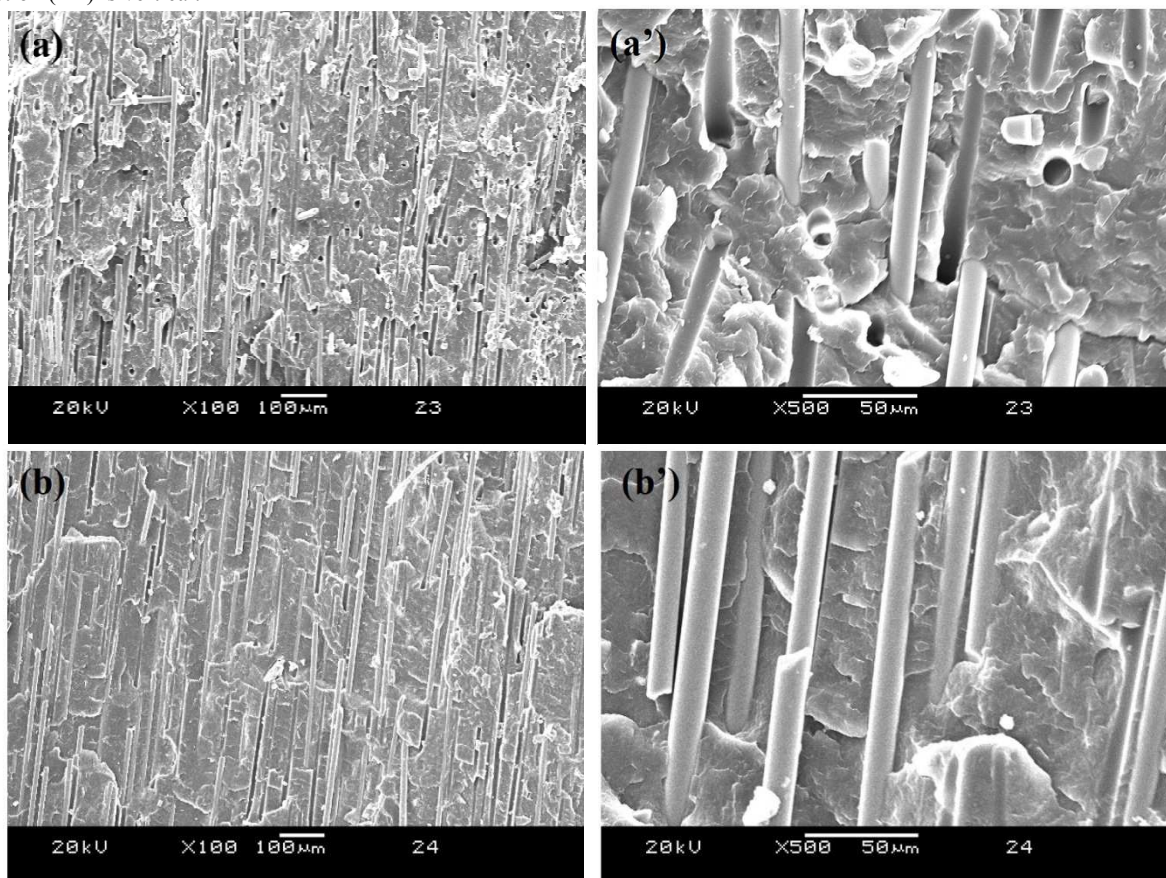


Fig. 6. SEM photographs of cryogenically fractured samples along FD. (a) and (a'), CIM β ; (b) and (b'), OSIM β . The shear flow direction (FD) is vertical.

ARTICLE

It was reported that the mechanical properties of injection-molded products could be reinforced by the orientation of glass fibers, which was governed by a set of processing conditions such as injection speed, melt and mold temperatures, flow and cooling rate.⁵⁴ It was also reported that fibers in the fiber filled polymer composites tended to align in the flow direction near the surface but exhibited a random distribution in the center during the CIM processing.^{54, 55} SEM observation was thus adopted to intuitively reveal the orientation of glass fibers in the OSIM β sample. Fig. 6 concentrates on the inner layer of CIM β and OSIM β samples. It is apparent that the glass fibers in the CIM β sample align irregularly in the iPP matrix, where most of glass fibers are oriented along the flow direction and others are oblique or oriented normal to the flow direction (Fig. 6a and 6a'), whereas the glass fibers in the counterpart are well aligned parallel to flow direction (Fig. 6b and 6b'). This further verifies that the orientation of the glass fibers is greatly enhanced by the OSIM processing. A higher shear velocity gradient existing in the OSIM processing is prone to increase the orientation of the adjacent melt layer, which leads to the enhanced orientation of glass fibers. This contributes to the increased tensile strength and modulus of OSIM samples.

During the OSIM processing, strong shear flow field given by two pistons moving reversibly is applied to the hot melt with β -nucleating agent in the mold. First of all, intense shear flow field encourages the alignment of molecular chains along the direction of the shear flow. In our case, the shear rate changes from several to ten thousands of s^{-1} (see the supplement information). Generally, only polymer molecules above the "critical orientation molecular weight" (M^*) could remain oriented after shear at a given shear rate ($\dot{\gamma}$), following the relationship $M^* \propto \dot{\gamma}^{-\alpha}$ where α is a positive exponent.⁵⁶ As $\dot{\gamma}$ increases, the small molecules with low molecular weight could be oriented, which become the constituents of shish-kebab structure. As a result, plentiful shish-kebabs are formed in the whole OSIM β sample. The intense shear flow does not stop until the gate of the mold is frozen. From then on, the sheared melt in the inner layer continues to crystallize under quiescent conditions, and at the same time, the oriented molecules or network starts to relax. Nevertheless, the rate of the relaxation of oriented molecules is greatly constrained by the partial frozen molecules and the fast crystallization, thus it just causes the slight reduction of the amount and size of shish-kebabs in the inner layer (Fig. 2, 3 and 5). Analogous to shear-induced shish-kebabs, the intense of shear flow field provided by the OSIM processing is also more favorable to highly orient the rigid glass fibers since the weaker shear flow in the CIM processing has been proved to orient the glass fibers along the direction of the shear flow in the outer layer in the GF/iPP parts.^{54, 55} Due to the absence of the intense shear flow, some oriented glass fibers also relax and exhibit irregular distribution in the inner layer (Fig. 5 and 6).

As for the absence of β -crystals in the outer layer of OSIM β sample (Fig. 2, 3 and 4), it is needed to be addressed here. In our previous work, it was observed that the content of β -crystals was relatively reduced under the coexistence of the

shear flow (shear rate: $30 s^{-1}$) and β -nucleating agent, compared with the sample only containing β -nucleating agent. It was found that the amounts of the nuclei for the growth of α and β -crystals were in the same order of magnitude, so that α and β -crystals competitively grew in the later stage of crystallization.⁵⁸ This is responsible for the decrease of β -crystals in the limited growth space. In this current case, more α -nuclei are created by the intense shear flow field and by the heterogeneous nucleation of the glass fibers, which results in the predomination of α -crystals rather than β -crystals in the outer layer. Therefore, β -crystals are completely suppressed in the outer layer. The increased content of β -crystals in the inner layer was ascribed to the decreased α -crystals caused by the declined shear flow. In fact, the content of β -crystals in the inner layer of OSIM β sample (0.224) is far below the content of β -crystals in the corresponding layer of CIM β sample (0.443), due to many unrelaxed α -crystal oriented precursors in the inner layer of OSIM β sample.

It has been well accepted that shish-kebabs as a self-reinforced structure can bring out notable reinforcement on iPP,^{57, 58} and fiber orientation is also favorable for reinforcement on glass fiber reinforced composites,^{54, 55} while β -crystals can greatly increase the toughness of glass fiber reinforced composites.³⁷ In this OSIM β sample, these factors are naturally combined with each other to form a specific hierarchical structure, as displayed in Fig. 7. Abundant self-reinforced shish-kebabs and highly oriented glass fibers are considerably present in the outer layer of the OSIM β sample, while in the inner layer the content of shish-kebabs slightly decreases and glass fibers are less oriented. There are scarcely β -crystals existing in the outer layer, while abundant β -spherulites are present in the inner layer. This schematic diagram can be verified by SEM observation, as shown in Fig. 8. This 'stiff skin and soft core' structure was similar to the hierarchical structure of plants in the natural world like bamboo or sugarcane. This bionic hierarchical structure was attributed to the excellent mechanical properties (Fig. 1). The tensile strength of the OSIM β sample give rise to an increase of 19.3 MPa compared to that of the CIM0 sample, while the impact strength of the OSIM β sample was increased by a factor of two times relative to that of the CIM0 sample. In addition, the tensile modulus rises from 2.1 to 2.80 GPa.

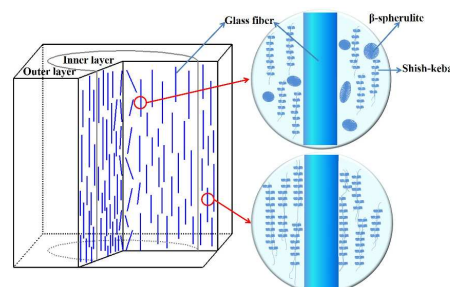


Fig. 7. Brief schematic diagrams of hierarchical structure of the OSIM β sample.

ARTICLE

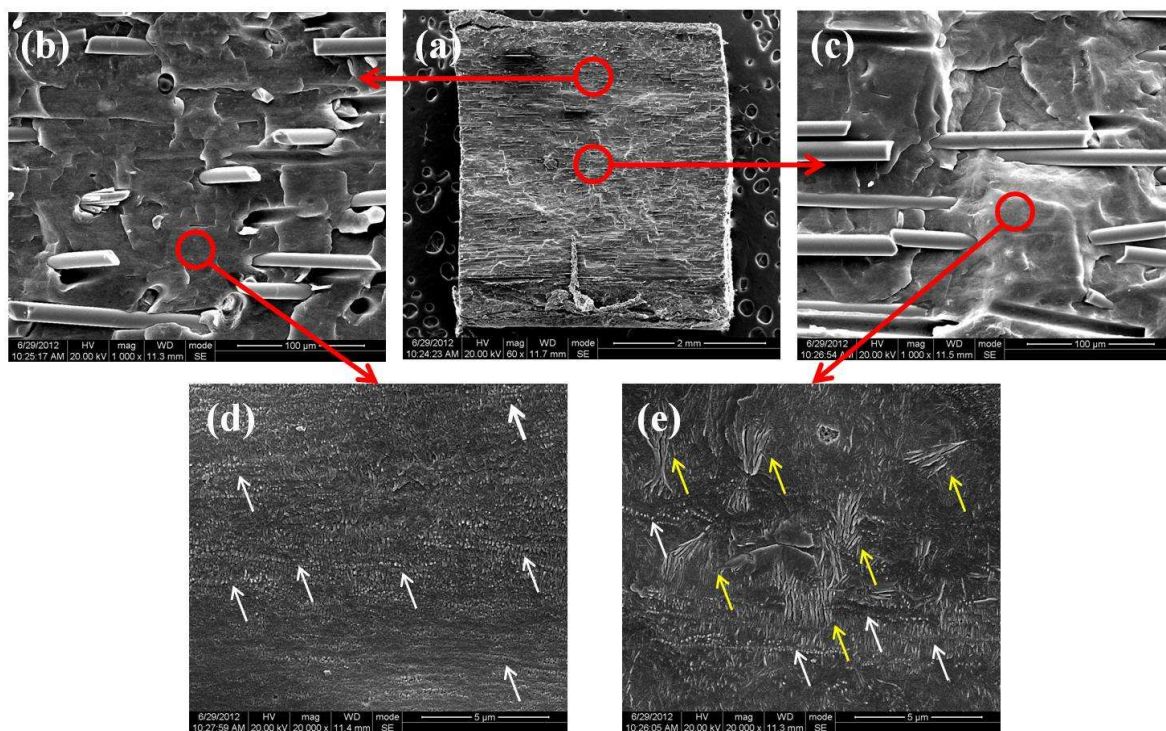


Fig. 8. (a) Full view of the OSIM β sample; (b) magnification of the skin layer of OSIM β sample; (c) magnification of the core layer of OSIM β sample; (d) further magnification of the skin layer of OSIM β sample; (e) further magnification of the core layer of OSIM β sample (white arrows indicate the shish-kebab structure and yellow arrows indicate the β -crystals). The shear flow direction (FD) is horizontal.

Conclusions

By combined usage of shear flow via the OSIM processing and addition of β -nucleating agent, we obtained a unique skin-core hierarchical structure in GF/iPP composites, similar to the structure in bamboo or sugarcane. It was found that highly oriented self-reinforced crystalline shish-kebabs and glass fibers were present in the outer layer, but a great deal of β -crystals were existed in the inner layer. The former structure led to the increase in strength and stiffness of the skin, while the latter (β -crystals in the inner layer) led to the increase in toughness. As a result, the OSIM β -nucleated GF/iPP composites exhibited simultaneously improved tensile strength and impact strength. Specifically, the tensile strength was increased by about 19.3 MPa and the impact strength exceeded two folds over those of CIM GF/iPP composites.

Acknowledgements

The authors gratefully acknowledge the financial support of this work by National Natural Science Foundation of China (Contract Number: 50925311, 51121001, 51120135002), the Innovation Team Program of Science & Technology Department of Sichuan Province (Grant 2013TD0013) and the

Doctoral Program of the Ministry of Education of China (Grant 20130181130012).

Notes and references

^a College of Polymer Science and Engineering and State Key Laboratory of Polymer Materials Engineering, Sichuan University, Chengdu 610065, China.

^b College of Chemical Engineering, Sichuan University, Chengdu 610065, China.

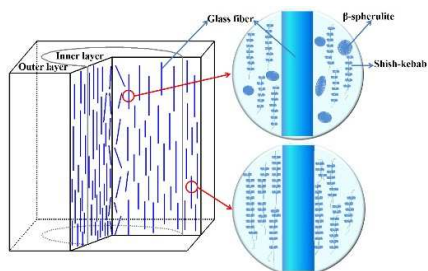
^c Department of Chemistry, Stony Brook University, Stony Brook, New York 11794-3400, USA.

* Corresponding authors. Tel./Fax: +86 28 85406866. E-mail address: zml@scu.edu.cn. Tel./Fax: +1 631 632 7793. E-mail address: bhsiao@notes.cc.sunysb.edu.

1. J. C. Wang, C. Z. Geng, F. Luo, Y. M. Liu, K. Wang, Q. Fu and B. B. He, *Mat Sci Eng a-Struct*, 2011, **528**, 3169-3176.
2. S. Panthapulakkal and M. Sain, *J Appl Polym Sci*, 2007, **103**, 2432-2441.
3. P. H. Foss, *Polym Composite*, 2004, **25**, 343-354.

4. Y. H. Chen, G. J. Zhong, Y. Wang, Z. M. Li and L. B. Li, *Macromolecules*, 2009, **42**, 4343-4348.
5. C. Valerio-Cardenas, A. Romo-Urbe and R. Cruz-Silva, *Polym Eng Sci*, 2011, **51**, 254-263.
6. S. L. Gao and E. Mäder, *Composites Part A*, 2002, **33**, 559-576.
7. K. S. Kumar, N. Bhatnagar and A. K. Ghosh, *Polym Composite*, 2008, **29**, 525-533.
8. S. Y. Fu, Y. W. Mai, B. Lauke, G. S. Xu and C. Y. Yue, *J Mater Sci*, 2002, **37**, 3067-3074.
9. J. L. Thomason and M. A. Vlug, *Composites Part A*, 1997, **28**, 277-288.
10. S. C. Tjong and S. A. Xu, *J Appl Polym Sci*, 2004, **94**, 1539-1546.
11. S. C. Tjong, S. A. Xu, R. K. Y. Li and Y. W. Mai, *Compos Sci Technol*, 2002, **62**, 831-840.
12. S. C. Tjong, S. A. Xu and Y. W. Mai, *J Polym Sci Part B Polym Phys*, 2002, **40**, 1881-1892.
13. D. Bikiaris, P. Matzinos, A. Larena, V. Flaris and C. Panayiotou, *J Appl Polym Sci*, 2001, **81**, 701-709.
14. D. Lariviere, P. Krawczak, C. Tiberi and P. Lucas, *Polym Composite*, 2004, **25**, 577-588.
15. E. Mader, S. L. Gao and R. Plonka, *Compos Sci Technol*, 2007, **67**, 1105-1115.
16. L. Mathew and R. Joseph, *J Appl Polym Sci*, 2007, **103**, 1640-1650.
17. V. Cech, *Compos Interface*, 2007, **14**, 321-334.
18. G. Jannerfeldt, R. Törnqvist, N. Rambert, L. Boogh and J.-A. E. Månson, *Appl Compos Mater*, 2001, **8**, 327-341.
19. X. Fu, B. B. He and X. Chen, *J Reinf Plast Comp*, 2010, **29**, 936-949.
20. S. H. Zhou, Y. Gao, Y. T. Wang, C. P. Hu and Q. Z. Dong, *J Appl Polym Sci*, 2007, **104**, 1661-1670.
21. A. T. Jones, J. M. Aizlewood and D. R. Beckett, *Die Makromolekulare Chemie*, 1964, **75**, 134-158.
22. S. Bruckner, S. V. Meille, V. Petraccone and B. Pirozzi, *Prog Polym Sci*, 1991, **16**, 361-404.
23. S. C. Tjong, J. S. Shen and R. K. Y. Li, *Scripta Metall Mater*, 1995, **33**, 503-508.
24. S. C. Tjong, J. S. Shen and R. K. Y. Li, *Polymer*, 1996, **37**, 2309-2316.
25. J. KargerKocsis, J. Varga and G. W. Ehrenstein, *J Appl Polym Sci*, 1997, **64**, 2057-2066.
26. S. C. Tjong, J. S. Shen and R. K. Y. Li, *Polym Eng Sci*, 1996, **36**, 100-105.
27. J. KargerKocsis and J. Varga, *J Appl Polym Sci*, 1996, **62**, 291-300.
28. D. R. Ferro, S. V. Meille and S. Bruckner, *Macromolecules*, 1998, **31**, 6926-6934.
29. H. B. Chen, J. Karger-Kocsis, J. S. Wu and J. Varga, *Polymer*, 2002, **43**, 6505-6514.
30. J. X. Li, W. L. Cheung and D. Jia, *Polymer*, 1999, **40**, 1219-1222.
31. C. Mathieu, A. Thierry, J. C. Wittmann and B. Lotz, *J Polym Sci Part B Polym Phys*, 2002, **40**, 2504-2515.
32. J. Varga and A. Menyhard, *Macromolecules*, 2007, **40**, 2422-2431.
33. A. J. Lovinger, J. O. Chua and C. C. Gryte, *J Polym Sci Polym Phys Ed*, 1977, **15**, 641-656.
34. J. Varga and J. KargerKocsis, *J Polym Sci Part B Polym Phys*, 1996, **34**, 657-670.
35. R. H. Somani, B. S. Hsiao, A. Nogales, H. Fruitwala, S. Srinivas and A. H. Tsou, *Macromolecules*, 2001, **34**, 5902-5909.
36. C. Grein, in *Intrinsic Molecular Mobility and Toughness of Polymers II*, ed. H.-H. Kausch, Springer Berlin Heidelberg, 2005, vol. 188, pp. 43-104.
37. H. Q. Xie, S. Zhang and D. Xie, *J Appl Polym Sci*, 2005, **96**, 1414-1420.
38. Y.-H. Chen, Y.-M. Mao, Z.-M. Li and B. S. Hsiao, *Macromolecules*, 2010, **43**, 6760-6771.
39. H. W. Bai, Y. Wang, Z. J. Zhang, L. Han, Y. L. Li, L. Liu, Z. W. Zhou and Y. F. Men, *Macromolecules*, 2009, **42**, 6647-6655.
40. G. J. Zhong, Z. M. Li, L. B. Li and E. Mendes, *Polymer*, 2007, **48**, 1729-1740.
41. A. Turner-Jones and A. J. Cobbold, *J Polym Sci Polym Part B Polym Lett*, 1968, **6**, 539-546.
42. Y. Mao, X. Li, C. Burger, B. S. Hsiao and A. H. Tsou, *Polymer*, 2013, **54**, 1432-1439.
43. H. Huo, S. C. Jiang, L. J. An and J. C. Feng, *Macromolecules*, 2004, **37**, 2478-2483.
44. R. H. Somani, L. Yang, B. S. Hsiao, T. Sun, N. V. Pogodina and A. Lustiger, *Macromolecules*, 2005, **38**, 1244-1255.
45. Q. Dou and O. L. Lu, *J Vinyl Addit Technol*, 2008, **14**, 136-141.
46. J. Cao, Z. Y. Zhao, R. N. Du, Q. Zhang and Q. Fu, *Plast Rubber Compos*, 2007, **36**, 320-325.
47. K. Trongtorsak, P. Supaphol and S. Tantayanon, *Polym Test*, 2004, **23**, 533-539.
48. G. Kumaraswamy, J. A. Kornfield, F. J. Yeh and B. S. Hsiao, *Macromolecules*, 2002, **35**, 1762-1769.
49. G. Kalay, Z. P. Zhong, P. Allan and M. J. Bevis, *Polymer*, 1996, **37**, 2077-2085.
50. P. W. Zhu, J. Tung and G. Edward, *Polymer*, 2005, **46**, 10960-10969.
51. N. Patil, L. Balzano, G. Portale and S. Rastogi, *Macromolecules*, 2010, **43**, 6749-6759.
52. W. Ruland, *Colloid Polym Sci*, 1977, **255**, 417-427.
53. N. Stribeck, Springer Berlin Heidelberg, Germany, 2007.
54. P. Gerard, J. Raine and J. Pabiot, *J Reinf Plast Comp*, 1998, **17**, 922-934.
55. C. F. Fan and S. L. Hsu, *J Polym Sci Part B Polym Phys*, 1989, **27**, 2605-2619.
56. L. Yang, R. H. Somani, I. Sics, B. S. Hsiao, R. Kolb, H. Fruitwala and C. Ong, *Macromolecules*, 2004, **37**, 4845-4859.
57. G. Kalay and M. J. Bevis, *J Polym Sci Part B Polym Phys*, 1997, **35**, 241-263.
58. B. A. G. Schrauwen, L. C. A. Von Breemen, A. B. Spoelstra, L. E. Govaert, G. W. M. Peters and H. E. H. Meijer, *Macromolecules*, 2004, **37**, 8618-8633.

Table of content



Glass fiber reinforced isotactic polypropylene composites with specific skin-core structure demonstrate simultaneous improvement of strength and toughness.